BEAM
INTERACTIONS
WITH
MATERIALS
AND ATOMS

Measurements of the total cross section of ^{nat}Be with thermal neutrons from a photo-neutron source

CrossMark

L.X. Liu [a,*], H.W. Wang [a,**], Y.G. Ma [a], X.G. Cao [a], X.Z. Cai [a], J.G. Chen [a], G.L. Zhang [a], J.L. Han [a,**], G.Q. Zhang [a], J.F. Hu [a], X.H. Wang [a,b], W.J. Li [a], Z. Yan [a], H.J. Fu [a,b,c]

[a] Shanghai Institute of Applied Physics, Chinese Academy of Sciences, Shanghai 201800, China
[b] University of Chinese Academy of Science, Beijing100080, China
[c] School of Materials Science and Engineering, Shanghai University, Shanghai 200444, China

A R T I C L E   I N F O

A B S T R A C T

The total neutron cross sections of natural beryllium in the neutron energy region of 0.007 to 0.1 eV were measured by using a time-of-flight (TOF) technique at the Shanghai Institute of Applied Physics (SINAP). The low energy neutrons were obtained by moderating the high energy neutrons from a pulsed photo-neutron source generated from a 16 MeV electron linac. The time dependent neutron background component was determined by employing the 12.8 cm boron-loaded polyethylene (PEB) (5% w.t.) to block neutron TOF path and using the Monte Carlo simulation methods. The present data was compared with the fold Harvey data with the response function of the photo-neutron source (PNS, phase-1). The present measurement of total cross section of ^{nat}Be for thermal neutrons based on PNS has been developed for the acquisition of nuclear data needed for the Thorium Molten Salt Reactor (TMSR).

1. Introduction

Beryllium, lithium and fluorine are the main nuclide of molten salt for the Thorium Molten Salt Reactor (TMSR) which is one of the six fourth generation reactors, such as 2LiF–BeF$_2$ coolant and LiF–BeF$_2$-ZrF$_4$-ThF$_4$-UF$_4$ fuel [1,2]. There are differences in the total cross sectional experiment data of beryllium in the thermal neutron energy region for a long time [3–7]. No additional experimental data has been added since 1989. Besides, there is a discrepancy of about 0.2 barn between the evaluation databases in the thermal neutron energy region. It directly affects the evaluation of nuclear data for other reaction channel. The thermal scattering effect is also very important for the calculation of reactor parameters. Therefore, it needs new measurement to improve the accuracy of evaluation data [8,9].

In the present work, the system for measuring the neutron total cross sections consists of a 16 MeV electron accelerator, water-cooled tungsten target (diameter is 60 mm and length is 48 mm) with a 10-cm-long polyethylene moderator, and 6.2-m-long flight path [10–12]. As a result of the limitation of experimental space,

the tungsten target chamber and the neutron detector were shielded to reduce the background. A combination utilizing 12.8 cm boron polyethylene (PEB) to block the neutron flight path and Monte Carlo methods was used to determine the time-dependent background component. A digital-signal-processing technique was used in the data acquisition of the system.

2. Experimental details

The PNS is a compact-type system for measuring the neutron total cross sections, and all its devices are arranged in the experimental hall in a 11 m × 8 m space, as shown in Fig. 1. Although it has the advantage of a small space, it has the disadvantage of a high neutron and γ-rays background. In order to reduce the neutron and γ-rays background, the tungsten target chamber is shield by 5 cm Al, 25 cm Pb, 15 cm polyethylene (PE), and 5 cm Al, in sequence. At the entrance of the electron beam, it is shield by 10 cm Al, 10 cm Pb, and 10 cm PEB. There is an L-type wall near the neutron detector, which consists of 30 cm concrete and 30 cm PEB. The TOF detector is shielded by 5 cm Fe and 30 cm PEB, and the monitor detector by 20 cm PEB.

A Pb plate with a thickness of 5 cm and a diameter of 10 cm was used to reduce the neutrons and γ-ray flash. A PE plate with a thickness of 10 cm and a diameter of 20 cm is used to increase the proportion of the thermal neutrons at PNS. A pulsed neutron
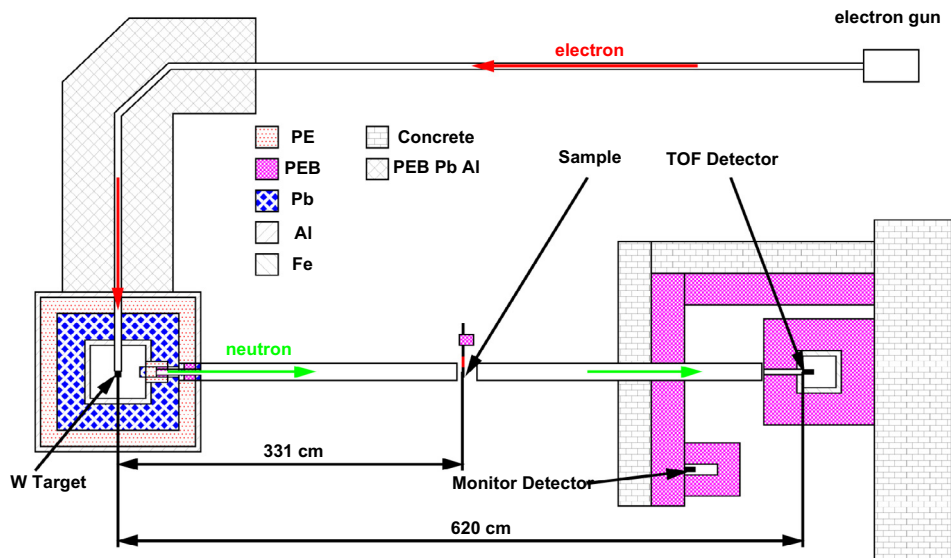
Fig. 1. Experimental geometry (plan view) of the PNS.

beam was collimated to a diameter of 5 cm by a 10 cm PEB tube, 15 cm Pb tube, 10 cm PEB tube, and 5 cm Pb tube, in sequence, as shown in Fig. 2.

The sample changer was located at 331 cm from the target. Five samples (including an open target) were held in the sample changer, which cycled at 300 s intervals. The first sample was a natural beryllium (^9Be) plate with a thickness of 10 mm, and 10×10 cm^2 in the cross-sectional area. The second sample was high-purity (99.995%) indium with a thickness of 0.1 mm (the data for this one is not discussed here, because it is irrelevant to this paper). The third sample was a set of notch filters of Cd (purity 99.99%) with 0.125-mm-thickness, Co (purity 99.9%) with 0.05-mm-thickness, Ag (purity 99.95%) with 0.1-mm-thickness, and In (purity 99.99%) with 0.05-mm-thickness plates. This sample was used

for energy calibration. The fourth sample was a PEB plate with a thickness of 12.8 cm for the background measurement. The last one was a blank sample. They all had the same size as that of the Be sample in the cross-sectional area. In the present experiment, the data were collected for 200 min for each sample.

A four channel waveform digitizer was used in this work. Channel 1 of the digitizer was the signal of the TOF detector, and channel 2 was the signal obtained by the Monitor detector. Channel 3 was the trigger signal (the electron GUN start signal) [13].

3. Simulation method

In order to obtain the response function and the time-dependent background component of this system, a Monte Carlo simulation code based on Geant4 was implemented. The version of Geant4 was Geant4.10.3 with G4NDL4.5, neutron data files with thermal cross sections.

Considering the calculation time, the local weighted method was used in the simulation. At the first step, particles with information on time, position, direction, energy, and type at position 1 (as shown in Fig. 2) were recorded in the simulation of the electrons from an electron tube with an energy of 16 MeV bombarding the tungsten target. At the second step, the particles recorded at position 1 were increased in number to continue the simulation. The number of neutrons detected by the TOF detector was approximately 14 counts in the simulation of electrons with 16 MeV, 10^{13} counts. It was approximately 39 counts with the same number of electrons in the experiment. From the comparison of these results, it was concluded that the physical list used in the simulation was reliable despite the uncertainty of the simulation being large due to low statistics.

In order to further reduce the computation time, the neutrons with information on time and energy at position 2 (as shown in Fig. 2) were recorded from the second step of the simulation. Then, the positions of the neutron source were chosen randomly at position 2, and the directions were all set to be parallel to the TOF tube at the third step of the simulation. The five different samples were all simulated as the experimental process, and the results of that were compared with the ones of the experiment, which are discussed in the next section.

In the simulation, we considered almost all factors influencing the measurements, such as the pulse width (1 μs), slowing time
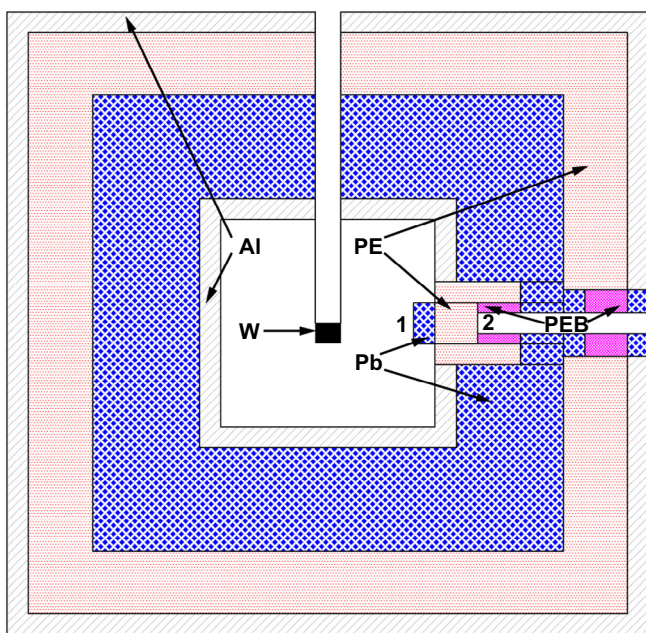

Fig. 2. Geometry (plan view) of the tungsten target chamber in the simulation. Position 1 is the left surface of the Pb plate with a diameter of 10 cm; Position 2 is the left surface of the neutron tube with a diameter of 5 cm.

of the target-moderator assembly, time precision of electronics, and geometrical factors.

4. Data analysis and results

The pulse-shape discrimination (PSD, calculated by using integral lengths) method was applied for n/γ identification for TOF spectrum calculations. The start signal for neutron TOF measurement was the falling edge of the electron GUN start signal and the stop signal was the neutron peak position of TOF detector [13].

4.1. Response function

$R(t_m, E)$ is the response function of a TOF-spectrometer. It is the probability, which a neutron with an energy E is measured with a time t_m [14]. The time t_m consists of several different independent components. In the case of the PNS facility the uncertainty in time is mainly from the neutron spend in the target-moderator assembly (t_t).

In order to determine the probability distribution of the time that the neutron transports in the target-moderator assembly, Monte Carlo simulations have been carried out for the PNS facility. Fig. 3 shows the response functions from the neutron transport in the target-moderator assembly of PNS. The distributions are for the neutrons collected at position 2 in Fig. 2. These distributions are strongly related to the neutron energy.

The equivalent distance L_t that a neutron transports in the target-moderator assembly can conveniently display the response functions of a TOF-spectrometer. The equivalent distance L_t is the product of v and t_t, and v is the velocity of the neutron when it comes out from the target-moderator assembly. The probability distributions of the equivalent distance L_t are shown in Fig. 4. The average equivalent distance and most probable distance is shown in Fig. 5. The most probable distance changes a little with the energy compared with the average equivalent one. The energy resolutions with the contribution due to the target-moderator assembly are shown in Fig. 6.

4.2. Background

The background in the TOF transmission measurement at PNS can be represented as follows

$$B(t) = B_0 + B_{no}(t) + B_{ns}(t) + B_{ne}(t). \tag{1}$$

The first time dependent component $B_{no}(t)$ originates from overlap neutrons that are measured but have been generated from a previous pulse. The component $B_{no}(t)$, which is related to the
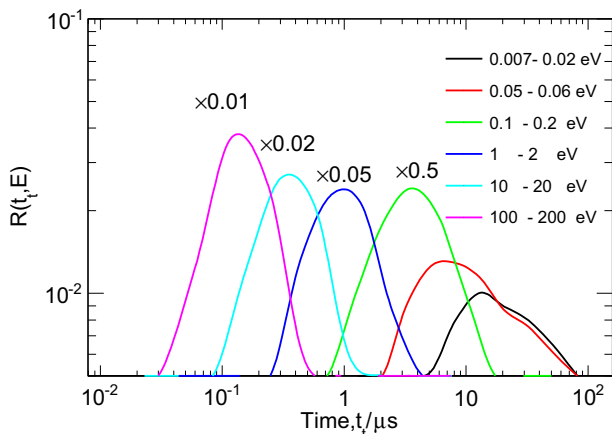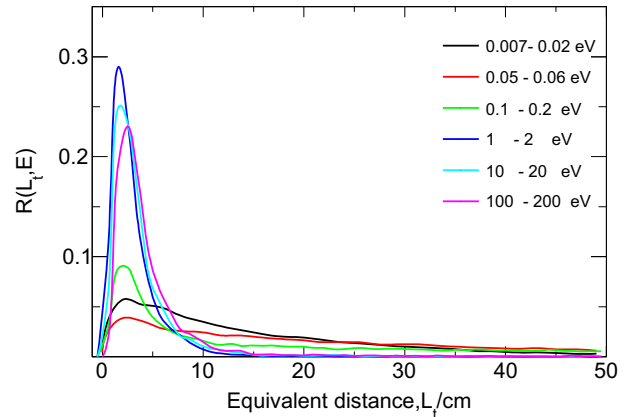

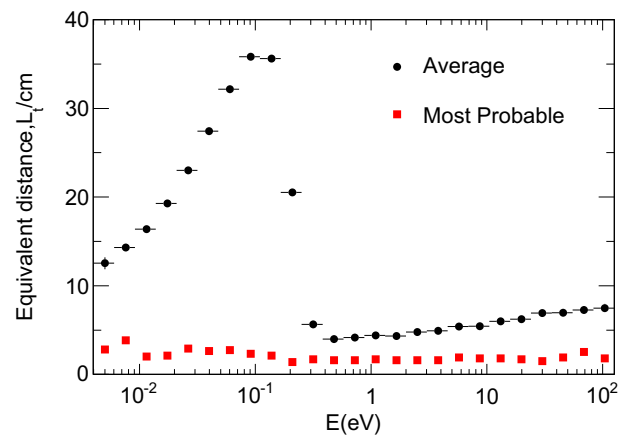**Fig. 4.** The probability distribution of L_t of PNS.

Fig. 5. The energy dependence of the average and most probable L_t for the target-moderator assembly of PNS.
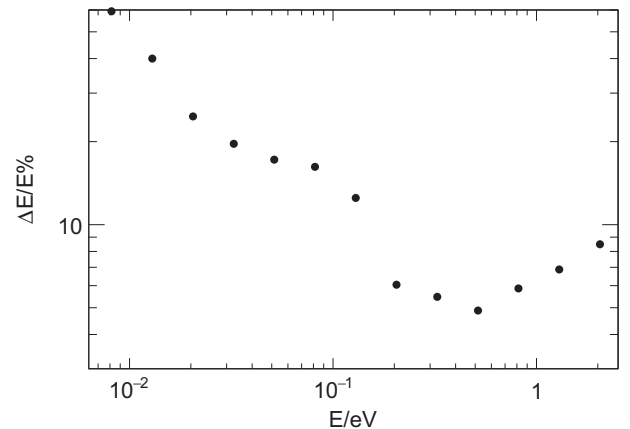

Fig. 6. The energy resolutions (at root-mean-square) for transmission measurements at PNS with the contribution due to the target-moderator assembly in the neutron energy range from 0.007 to 2 eV.

operating frequency of the accelerator, can be neglected at a low frequency. A second time dependent component $B_{ns}(t)$ is due to beam neutrons scattered inside the TOF detector shield. The $B_{ns}(t)$ of the open target and Be sample by simulation are shown in Fig. 7. A third time dependent component $B_{ne}(t)$ results from neutrons scattered in the environment. It is hard to make a
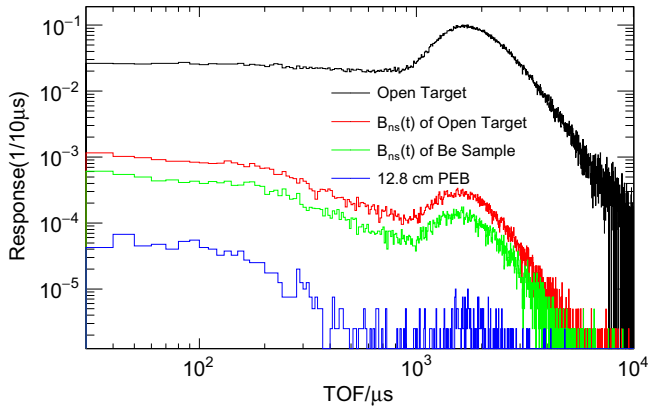

Fig. 3. The probability distribution of t_t of PNS.

Fig. 7. The response of the neutron detector by simulation: the $B_{ns}(t)$ background of the open target, Be sample, and the TOF spectrum of the neutrons transmitted through 12.8 cm PEB.

distinction between the time independent background B_0 and the time dependence background. The total contribution $B_0 + B_{ne}(t)$ could be determined by the method with the beam blocked.

The $B_0 + B_{ne}(t)$ background level was estimated by using the background sample with 12.8-cm-thick PEB. The TOF spectrum of the neutrons transmitted through PEB is shown in Fig. 7. This proved that the $B_0 + B_{ne}(t)$ background level in Fig. 8 is reliable. It was also proved to be accurate by the neutron TOF spectrum for the notch filter of 0.05 mm Co, 0.1 mm Ag, 0.05 mm In, and 0.125 mm Cd samples in Fig. 8. The dip of Co was not enough deep because of the transmission rate and $B_{ns}(t)$, as shown in Fig. 7. The transmission rates of Co, Ag, and In were approximately 0.009, 3×10^{-7}, and 8×10^{-6}, respectively.

In Fig. 9, the TOF spectra for the open target and notch filter of the experiment have subtracted background. The TOF spectra for the open target and notch filter of the experiment were consistent with the ones obtained by the simulation in the time and shape, except for some differences in the number of counts in the lower time region.

4.3. Total cross section

The neutron total cross section is related to the transmission rate, which is the fraction of neutrons transmitted through a sample compared to that transmitted without sample. The relation between the neutron total cross section $\sigma_T(E_i)$ and the transmission rate at the ith bin energy E_i is as follows:

$$T(E_i) = \frac{[S(E_i)/M_S - B_S(E_i)/M_{B_S}]}{[O(E_i)/M_O - B_O(E_i)/M_{B_O}]}, \tag{2}$$

Table 1
Resonance time of the corresponding neutron energy.

Isotope	Resonance energy/eV	Experiment/μs	Simulation/μs
^{59}Co	132.0	39.50	37.22
^{109}Ag	5.19	189.72	188.14
^{115}In	1.457	355.23	353.29

Table 2
Flight path length and time difference.

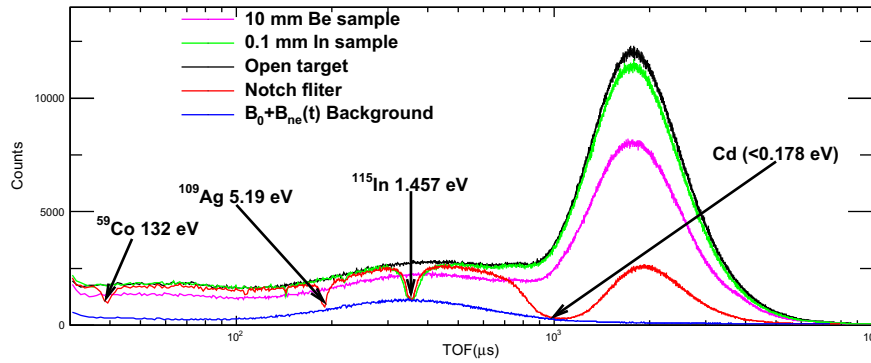|	Effective length/m	τ_0/μs
Experiment	5.903 ± 0.004	2.36 ± 0.03
Simulation	5.928 ± 0.010	−0.09 ± 0.06

Fig. 8. Experimental TOF spectra for the Be sample, In sample, open target, notch filter, and $B_0 + B_{ne}(t)$ background.
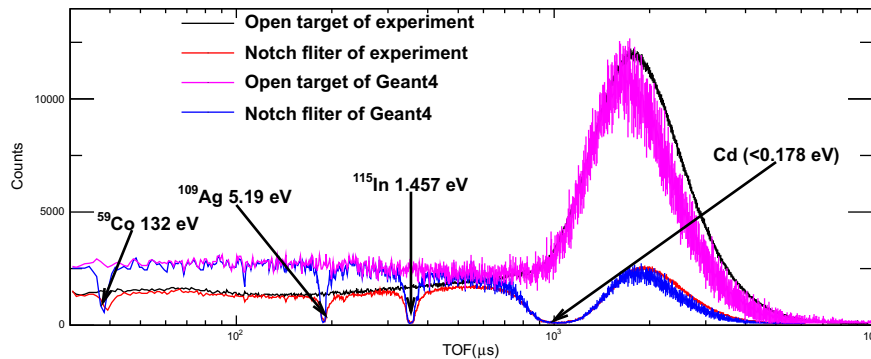

Fig. 9. TOF spectra for the open target and notch filter with the $B_0 + B_{ne}(t)$ background subtracted of the experiment compared with those obtained by the simulation.
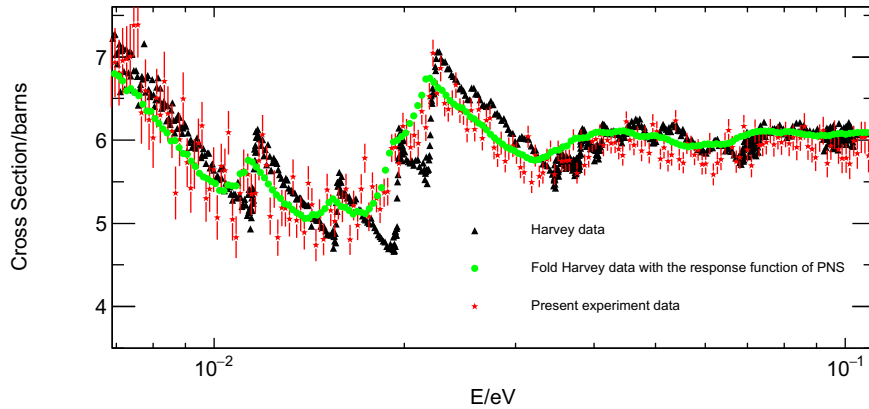
Fig. 10. Neutron total cross section of beryllium compared with the Harvey data and the fold Harvey data with the response function of PNS.

$$\sigma_T(E_i) = -\frac{1}{N} \ln T(E_i), \tag{3}$$

where $S(E_i)$ is the count of the sample with a thickness of N atoms per barn, $O(E_i)$ is the blank sample count, $B_S(E_i)$ is the background count of the sample, and $B_O(E_i)$ is the background count of the blank sample. M_S, M_O, M_{B_S} and M_{B_O} are the normalized constants according to the monitored counts of the three samples. $S(E_i), O(E_i), B_S(E_i)$ and $B_O(E_i)$ are all normalized to the counts of $O(E_i)$ through the three normalized constants.

The resonance times of Co, Ag, and In were determined by fitting the absorption peak as a function of TOF by using the following fitting function,

$$y = C_0 + C_1 t - (2A/\pi)w/[4(t-t_c)^2 + w^2], \tag{4}$$

where C_0 is the starting neutron count, C_1 is the slope, A is the area of the absorption peak, w is the width of the peak, and t_c is the position of the peak, i.e. the resonance time. All the results are summarized in Table 1.

The flight path length L was obtained from the resonance energy E_n in electronvolts corresponding to the channel number I of the resonance time as indicated in Table 1 by using the following fitting function,

$$E_n[eV] = (72.3 \times L[m]/(I \times \Delta W - \tau_0)[\mu s])^2, \tag{5}$$

where ΔW is the channel width of the digitizer, which is 4 ns and τ_0 is the time difference between the start time from the accelerator trigger and the real time zero when the neutron was generated. L and τ_0 of both experiment and simulation are shown in Table 2. L of the simulation agreed well with that of the experiment with a little difference. The electron source in the simulation was set at 8 cm from the front surface of the target, so τ_0 of the simulation was close to zero. The accelerator trigger of the experiment was delayed.

The total cross sections of beryllium were obtained in the neutron energy range from 0.007 to 0.1 eV by using Eqs. 2 and 3, as shown in Fig. 10. The statistical uncertainty can be determined from Eq. 3 if it's assumed that the monitor counters are constant during the experiment as follows:

$$(\Delta\sigma_{stat.})_i = \frac{1}{N}\sqrt{\frac{S(E_i)/M_S + B_S(E_i)/M_{B_S}}{[S(E_i)/M_S - B_S(E_i)/M_{B_S}]^2} + \frac{O(E_i)/M_O + B_O(E_i)/M_{B_O}}{[O(E_i)/M_O - B_O(E_i)/M_{B_O}]^2}}, \tag{6}$$

where subscript i corresponds to each energy bin, as in reference [15]. The total statistical uncertainties for the measured total cross sections are varied from 2% to 6% as a function of the neutron energy.

The present measurement is shown to be in excellent agreement with the fold high-accuracy measurement performed by Harvey et al. [7] with the response function of PNS in the energy range from 0.007 to 0.1 eV, as shown in Fig. 10. It demonstrates that the uncertainties of the measurements at PNS are primarily due to the uncertainty in time by the neutron spends in the target-moderator assembly. Fig. 10 also shows the total cross section data from Harvey is better than the present measurement. Its main reason is the neutron energy precision caused by flight length and target-moderator assembly. In addition, the statistical uncertainty is also one of the reasons.

5. Conclusion

A system for measuring the total thermal neutrons cross section was described in this paper. The digital-signal-processing technique and a background measurement method were used in the system. The energy resolutions due to the target-moderator assembly were obtained by using a Geant4 simulation. In order to decrease the calculation time, the local weighted method was used in the simulation. The neutron total cross section for beryllium was measured by this system in the range from 0.007 to 0.1 eV and compared with that of the fold Harvey data. The statistical uncertainties are varied from 2% to 6% as a function of the neutron energy.

References

[1] R.M. Ji, M.H. Li, Y. Zou, G.M. Liu, Nucl. Sci. Tech. 28 (6) (2017) 76.
[2] C. Peng, X.W. Zhu, G.Q. Zhang, Z.Z. He, K. Chen, Nucl. Sci. Tech. 27 (2) (2016) 44.
[3] L.J. Rainwater, W.W. Havens jr, Chicago University Metall. Labs Rep. 2269 (1944).
[4] V.P. Duggal, C.L. Thaper, Rev. Sci. Instrum. 33 (1962) 49.
[5] V.F. Gerasimov, Y.S. Zenkevich, S.S. Moskelev, D.A. Markov, A.V. Kheruvimov, Inst. Atomnoy Energii, Kurchatov Rep. 2222 (1972).

[6] K. Kanda, O. Aisawa, J. Nucl. Sci. Technol. 12 (10) (1975) 601–605.
[7] J.A. Harvey, H.A. Mook, N.W. Hill, O. Shahal, Nucl. Data Sci. Technol. (1982) 961–964.
[8] Z.D. Wu, H.Y. Liang, Y.L. Han, Nucl. Sci. Tech. 27 (4) (2016) 102.
[9] C.L. lan, M. Peng, Y. Zhang, Z. Wei, Z.E. Yao, B.L. Xie, Nucl. Sci. Tech. 28 (1) (2017) 8.
[10] M.H. Jiang, H.J. Xu, Z.M. Dai, Bull. Chinese Acad. Sci. 27 (3) (2012) 366–374.
[11] Z.K. Lin, G.M. Sun, J.G. Chen, G.M. Liu, Z.M. Dai, Nucl. Sci. Tech. 23 (2012) 272–276.
[12] Z.K. Lin, X. Zou, Y. Cao, Z.M. Dai, At. Energy Sci. Technol. 46 (2012) 26–30.
[13] L.X. Liu, H.W. Wang, Y.G. Ma, X.G. Cao, X.Z. Cai, J.G. Chen, G.L. Zhang, J.L. Han, G. Q. Zhang, J.F. Hu, X.H. Wang, Chinese Phys. C 40 (5) (2016) 056202.
[14] P. Schillebeeckx, B. Becker, Y. Danon, K. Guber, H. Harada, J. Heyse, A.R. Junghans, S. Kopecky, C. Massimi, M.C. Moxon, N. Otuka, I. Sirakov, K. Volev, Nucl. Data Sheets 113 (2012) 3054–3100.
[15] T.F. Wang, M.W. Lee, K.S. Kim, G.Y. Kim, Y.D. Oh, M.H. Cho, I.S. Ko, W. Namkung, T.I. Ro, Nucl. Instruments Methods Phys. Res. B 268 (2010) 106–113.